Supramolecular cooperativity through the lens of enhanced sampling molecular dynamics

RESEARCH ARTICLE | JANUARY 23 2026

Supramolecular cooperativity through the lens of enhanced sampling molecular dynamics

Special Collection: Michele Parrinello Festschrift

A. Cardellini ; D. Polino ; C. Perego

J. Chem. Phys. 164, 044904 (2026)
https://doi.org/10.1063/5.0288284

The Journal of Chemical Physics ARTICLE pubs.aip.org/aip/jcp

Supramolecular cooperativity through the lens of enhanced sampling molecular dynamics

Cite as: J. Chem. Phys. 164, 044904 (2026); doi: 10.1063/5.0288284
Submitted: 30 June 2025 • Accepted: 31 December 2025 •
Published Online: 23 January 2026

A. Cardellini,[1] D. Polino,[1] and C. Perego[1,2,a)]

AFFILIATIONS

[1] Department of Innovative Technologies, University of Applied Sciences and Arts of Southern Switzerland, Polo Universitario Lugano, Campus Est, Via la Santa 1, 6962 Lugano-Viganello, Switzerland
[2] Department of Applied Science and Technology, Politecnico di Torino, Corso Duca degli Abruzzi 24, 10129 Torino, Italy

Note: This paper is part of the JCP Special Topic, Michele Parrinello Festschrift.
[a)]**Author to whom correspondence should be addressed:** claudio.perego@polito.it

ABSTRACT

Supramolecular polymers are dynamic aggregates whose properties arise from their constitutive bonds, based on reversible, non-covalent interactions. A central aspect in the design and function of these materials is the cooperativity of polymerization, by which the addition of monomers becomes increasingly favorable as the polymer grows. Cooperativity strongly influences both the structure and collective behavior of supramolecular materials, with significant implications for their properties. Understanding the origins and consequences of cooperativity is crucial for the rational design of new functional supramolecular polymer systems. Herein, we systematically explore the cooperativity of supramolecular polymer systems via Molecular Dynamics simulations, powered by On-the-fly Probability Enhanced Sampling, to accurately characterize the free energy landscape associated with polymerization. We validate our approach via ad hoc, minimalistic coarse-grained models of cooperative and non-cooperative self-assembling monomers. We then apply our analysis to ureidopyrimidinone (UPy) supramolecular polymers, widely used in biohydrogel design. Our work provides detailed insights into the UPy polymerization process and how cooperativity can emerge from the hierarchical character of its supramolecular structure. The results underscore the importance of an extensive molecular simulation approach to obtain a quantitative characterization of the self-assembly thermodynamics, which is crucial to guide the rational development of next-generation supramolecular materials.

I. INTRODUCTION

Supramolecular polymers (SPs) are formed by molecular units that self-assemble via noncovalent interactions (H-bonds, π–π stacking, and metal coordination).[1–3] Built upon reversible, dynamic bonds, SPs exhibit properties such as self-healing and stimuli-responsiveness,[4–7] bearing potential for applications in smart and biomaterial engineering.[8–14] A crucial aspect in SP design concerns the mechanism of polymerization. Based on the free energy balance associated with the formation of differently sized assemblies, SP polymerization has been classified as *isodesmic* or *cooperative*.[15–21] In the former case, the equilibrium constant of polymerization does not depend on the assembly size, while in cooperative SPs, the equilibrium constant changes with size. In cooperative systems, the polymerization of small oligomers is characterized by a smaller association constant with respect to the growth of long stacks. This entails an activated mechanism of nucleation/elongation, in which the slow nucleation of critical-size polymers is followed by rapid growth.[3,16,22] In some cases, dubbed "anti-cooperative,"[23–25] the association constant of elongation (aggregation/growth of long stacks) is instead smaller than that of nucleation (aggregation/growth of small constructs).

Cooperativity has implications for the structure and dynamics of supramolecular polymer systems, for example, by determining higher monodispersity of aggregates,[19,26] high sensitivity to external conditions and stimuli,[27,28] hysteresis,[29,30] kinetic trapping,[22,31] and more. These are crucial features in guiding the design of new SP-based materials, which is why understanding the phenomenon of cooperativity in depth is of primary importance. Experiments allow for detecting the key signatures of cooperativity[18,22,32,33] and

for identifying the global drivers of polymerization.[34–41] However, the detail accessible by state-of-the-art diagnostics is typically insufficient to isolate which molecular factors impart cooperativity in a system.

Molecular Dynamics (MD) simulations are a key tool in the study of SPs, as the scales of polymerization are compatible with those accessed by classic All-Atom (AA)[42–44] and Coarse-Grained (CG) MD.[45–47] MD allows reproducing polymerization with precise control of the assembly size, characterizing the intermolecular interaction landscape that is responsible for cooperativity. Several MD studies on, e.g., benzene-1,3,5-tricarboxamide (BTA) SPs have underlined crucial factors of their supramolecular structure and dynamics,[21,48–50] including quantitative signatures of their cooperative polymerization.[21,47,50,51] MD investigation was extended to other SP systems, typically supporting and complementing experimental evidence.[33,52–55] However, accurately estimating the free energy balance associated with supramolecular polymerization, which defines cooperativity, remains a non-trivial task for which enhanced sampling becomes necessary.[21,47,56,57] We here propose an MD approach, based on the recent On-the-fly Probability Enhanced Sampling (OPES) method,[58] to evaluate how the thermodynamics of SP polymerization depends on the size of interacting aggregates. We first outline and validate our strategy by comparing the free energy landscapes of prototypical SP systems, represented by simple, minimalistic CG models designed to self-assemble either via an isodesmic or cooperative process.[54,59]

We then employ the developed strategy to explore how cooperativity emerges in a real SP system, formed by ureidopyrimidinone (UPy) molecules that self-organize in "hierarchical" fibrillar structures.[60–62] UPy monomer variants are a paradigmatic example of SP building blocks, of high relevance due to their tunability and potential biocompatibility.[63] The mechanical and dynamic features of UPy polymers are crucial for engineering biomimetic hydrogels[64,65] toward the synthetic reproduction of extracellular matrix adaptive properties.[64,66–68] We recently investigated UPy-based SPs in water using AA-MD simulations combined with Well-Tempered MetaDynamics,[69] observing how monomers travel across the supramolecular structure of such a system.[70] We here advance our understanding of this SP system by assessing and quantifying the cooperativity of UPy polymerization, both in chloroform and water. The use of an advanced enhanced sampling approach allows a very accurate characterization of the UPy polymerization landscape, showing how different aggregation modes combine, giving rise to a cooperative polymerization process.

II. RESULTS

The cooperativity of supramolecular polymerization is defined by the dependence of the equilibrium association constant K on the size of the aggregates involved in the process.[3,71] In a noncooperative, *isodesmic* system, the end groups interact independently of the size of the polymer to which they belong, so the system is characterized by a single, size-invariant association constant. In *cooperative* systems, the association constant has at least two different values depending on the size of the interacting oligomers: K_n, for aggregation at sizes lower than the critical one, and $K_e > K_n$, for larger sizes. This defines a slower nucleation stage followed by an elongation stage in which association is favored.[3,71] This is the simplest realization of cooperativity, but in general, we expect K to keep changing along the aggregation route.

Cooperative systems differentiate from isodesmic ones by collective structural signatures, showing, for example, a bimodal size distribution, as opposed to the unimodal isodesmic one, or qualitatively different behavior of volume fraction and polymerization degree with temperature and concentration.[3,72,73] Whereas these structural features can be detected by experiments,[30,74] they do not reveal which molecular or chemical features give rise to such association behavior. Computational studies, both via simple kinetic association models[31,73–76] or via minimalistic MD models,[51,53,54,59] have allowed the bridging of molecular-level information with the collective fingerprints of cooperative polymerization. However, when realistic molecular systems are considered, a quantification of cooperativity becomes extremely challenging, due to the limited space and time scales accessible via molecular simulations and due to the complexity of the self-assembling process.[77,78]

We herein adopt a protocol in which different polymerization steps are considered separately, and the conditional free energy difference associated with each step is computed via the OPES method.[58] The association constant $K_{n,m}$ of an n-mer with an m-mer is related to the conditional free energy difference $\Delta G_{n,m}$ of that polymerization step by

$$\Delta G_{n,m} = -k_B T \log K_{n,m}, \tag{1}$$

where k_B is the Boltzmann constant and T the temperature. Evaluating the ΔG associated with the main polymerization steps enables a detailed, quantitative insight into the aggregation routes, allowing us to rationalize and quantify cooperativity. To compute the free energy differences, we here rely on the OPES method,[58] which applies a history-dependent bias potential along properly selected collective variables (CVs), adapted on-the-fly according to the estimated probability distribution. OPES is employed to extensively sample the binding and unbinding of oligomers of controlled size n and m (controlled via restraining potential, see Sec. IV), allowing an accurate estimate of $\Delta G_{n,m}$.

Notably, a strategy based on the calculation of conditional ΔG values was applied by Korlepara *et al.* in Ref. 21, combined with the Adaptive Biasing Force method[79] to drive the association of a monomer onto different-sized oligomers for two 1D SPs, that is, a [2.2]paracyclophane-tetracarboxamide derivative and benzene-1,3,5-tricarboxamide. However, most often SP aggregation pathways are more complex than in standard monodirectional polymerization, as, for example, when an assembly is mediated by a fuel,[9,80] or when a hierarchical structure is formed,[81–83] as in the UPy SPs considered herein.[61,64,68] Therefore, in general, the landscape of reaction variables can reach higher dimensionalities, a ground in which the OPES method is in principle more competitive than a force-based approach.[84,85] Our choice of OPES is therefore motivated toward a general enhanced sampling approach of the polymerization landscape, capturing the main factors that contribute to cooperativity in supramolecular systems.

We first test this approach using two prototypical minimalistic CG models,[59] that is, simple, implicit solvent molecular models designed to reproduce only essential details of self-assembly.[53,54] The first model, **M**, is composed of planar monomers, each formed

by a core bead surrounded by lateral beads at the vertices of a hexagon. Harmonic bonds maintain the monomer planar, while Lennard-Jones (LJ) potentials between the beads regulate intermolecular interactions. Specifically, the core beads interact with each other via a strong LJ potential (ε = 45 kJ/mol), while the lateral beads have much weaker interactions ($\varepsilon_{\text{lateral}}$ = 0.2 kJ/mol), acting as excluded-volume centers. As a result, monomers aggregate along the axial direction driven by the LJ attraction between the core beads (see Sec. IV and Refs. 54 and 59 for further details). The short-range binding forces in the **M** model should not be affected by polymer size; therefore, we expect this model to follow isodesmic polymerization (as also shown in Ref. 59).

The second test case, named $\mathbf{M}_{\text{coop}}$, is based on the same molecular shape as the **M** model, having a lower core–core interaction ($\varepsilon_{\text{coop}}$ = 20 kJ/mol)) and the addition of a freely rotating dipole anchored at the center of the core. Such a dipole is formed by two oppositely charged material points, restrained along a vector [Fig. 1(A)]. The electrostatic interaction between these charges complements the LJ attraction between the core beads, determining a system that aggregates following a cooperative mechanism[59] (see Sec. IV for further details), guided by the additional degrees of freedom of the dipole vectors. The charges and LJ interaction parameters have been tuned to obtain a similar propensity to aggregation in the **M** and $\mathbf{M}_{\text{coop}}$ models at at T = 300 K,[59] so that the comparison between isodesmic and cooperative polymerization is more straightforward.

We here apply our OPES-based approach to quantitatively characterize the thermodynamics of aggregation of these two models, showing how the different intermolecular interactions give rise to diverging polymerization pathways. We computed the free energies associated with the elementary polymerization steps that lead from the monomeric to the polymeric state. Being in a constant-volume ensemble, we here compute the Helmholtz free energy differences associated with the process $\Delta F_{n,m}$, instead of the Gibbs

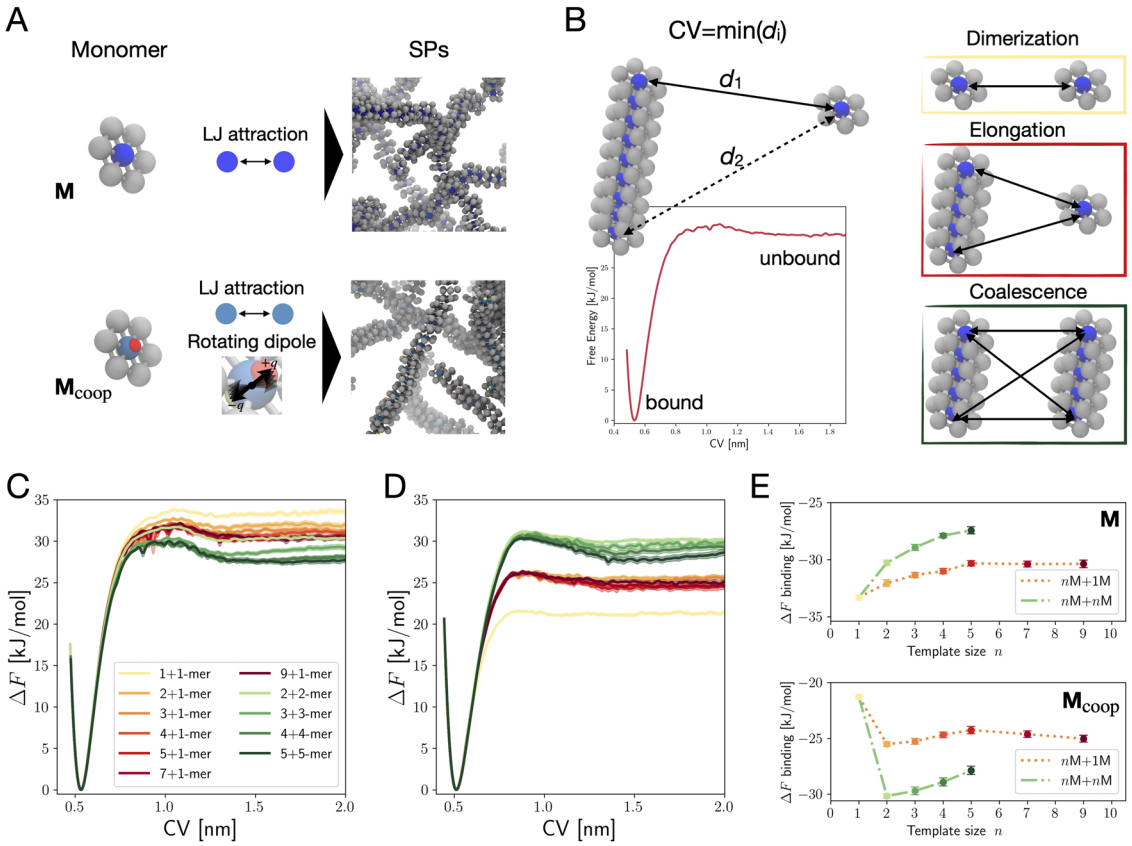

FIG. 1. Cooperativity of minimalistic CG SP models. (A) **M** model (top) and $\mathbf{M}_{\text{coop}}$ model (bottom). The **M** monomer polymerizes via LJ attraction between the central, core beads (blue). The $\mathbf{M}_{\text{coop}}$ model (bottom) polymerizes via the combination of LJ attraction between the core beads (green–blue, weaker than in **M**) and electrostatic interaction between the rigid rotating dipoles (red and yellow beads are positive and negative charges). (B) The OPES bias potential is applied using the minimum core–core distance between interacting ends as a CV, obtaining the typical free energy profile shown in red. We evaluate the free energy of the following polymerization steps: dimerization (1 + 1-mer), polymer elongation (n+ 1-mer) and polymer coalescence (n + n-mer). (C) Free energy profiles associated with the **M** model. The minimum is shifted to 0. Shaded areas indicate the error (see Sec. IV). (D) Free energy profiles associated with the $\mathbf{M}_{\text{coop}}$ model, same legend as C. The minimum is shifted to 0. Shaded areas indicate the error (see Sec. IV). (E) Free energy differences associated with binding (i.e., $\Delta F = F_{\text{bound}} - F_{\text{unbound}}$) for the different polymerization steps for the **M** (top) and $\mathbf{M}_{\text{coop}}$ (bottom) models.

free energy $\Delta G_{n,m}$. As shown in Fig. 1(B), we consider three classes of polymerization steps: dimerization, that is, the binding of two monomers (1 + 1-mer); elongation, that is, the binding of a monomer to an oligomer of size n (n + 1-mer); and coalescence, that is, the binding of two oligomers ($n + n$-mer, we assume only same-size oligomers for simplicity). We do not consider here polymerization steps that imply intercalation of molecules within the backbone of an existing construct, or branching of polymers, based on evidence that such processes have a relatively negligible incidence.[59] As the CV for the OPES method, we chose the minimum distance between the geometric centers of the reactive ends of the two associating oligomers. Harmonic restraints have been employed to restrict the sampling to the selected polymerization step, as discussed in Sec. IV.

The free energy profiles associated with each of the considered polymerization steps are shown in Fig. 1(C) for the **M** system and in Fig. 1(D) for the $\mathbf{M}_{\text{coop}}$ system. It is evident that the free energies follow qualitatively different trends in the two systems [Fig. 1(E)]. In the **M** model, the ΔF magnitude slightly decreases with the size of the involved constructs. Dimerization has the largest $|\Delta F|$, whereas elongation steps show slightly lower $|\Delta F|$s, which seem to saturate as the size of the polymer increases. The size dependence of ΔF is then further accentuated when coalescence is considered. As the binding interactions involved in the model are size-independent by design, this slight ΔF size dependence could be of entropic origin. Indeed, the loss of rotational and translational entropy associated with binding can introduce a free energy penalty when larger constructs are involved. We support this hypothesis by computing the internal energy and entropy differences associated with the polymerization steps (see supplementary material, Fig. S1), showing that the size dependence is entropy driven.

The free energy differences detected in the $\mathbf{M}_{\text{coop}}$ system show an opposite dependence on the size of the involved constructs. The smallest $|\Delta F|$ is associated with dimerization, while increased free energy variations are found for elongation and coalescence steps, with the latter being more favored. This demonstrates and quantifies the cooperative behavior of the model. Interestingly, ΔF clearly differentiates between the three classes of polymerization steps, rather than across different sizes. All elongation steps show the same free energy difference, while coalescence steps display only a slight dependence on size, with smaller magnitudes of $|\Delta F|$ for larger n. This indicates that the key steps determining the cooperativity of this model are essentially two, related to the change in dipole configuration: (i) a free monomer's dipole becomes part of a polymer terminal, and (ii) a dipole at the terminal of a construct binds to another one, becoming part of a polymer backbone. Step (i) is involved in dimerization and elongation, while step (ii) is involved in elongation and coalescence. The results of Fig. 1(E) suggest that step (ii) entails the largest free energy drop, determining the differences between the computed ΔFs. Similarly to what occurs in the **M** model, the weak size dependence exhibited by coalescence free energies can be attributed to the entropic cost of binding larger constructs (see Fig. S1). Furthermore, this analysis reveals that the free energy gain associated with elongation and coalescence is mostly driven by the internal energy ΔE, rather than entropy.

Overall, our approach enables an accurate characterization of the thermodynamics of polymerization in both systems, also revealing aspects that, despite the simplicity of the models, are otherwise inaccessible.

The results obtained with the test case of minimalistic isodesmic and cooperative CG models stimulate the use of our OPES-based approach with the more complex case of UPy SPs. We here look at the most basic form of the UPy monomer, that is without any additional side group [Fig. 2(A)], to focus on the aggregation drivers of the UPy core without interference from side groups (see Sec. IV for details on the AA model). Details on the possible impact of side chains are reported in the supplementary material (Fig. S3), showing that functionalizing the UPy monomer with a hydrophobic tail and an additional urea group does not necessarily lead to the formation of a well-defined 1D SP, as also confirmed experimentally.[86]

As known from experimental[60,61,87] and computational[70] evidence, the UPy motifs form SPs by a hierarchical aggregation process, which combines two binding modes [Fig. 2(A)]. On the one hand, UPy cores can form planar dimers by the combination of 4 complementary hydrogen bonds, in a donor–donor–acceptor–acceptor (DDAA) arrangement.[60,61] On the other hand, the aromatic UPy cores can stack along the normal direction.[61,88] The combination of these two binding modes gives rise to 1D polymeric assemblies, as shown in Fig. 2(B), which constitute the fundamental structure of UPy SP networks.[61,64] To support the formation of such polymeric aggregation, we performed self-assembly AA-MD simulations starting from dispersed UPy motifs in apolar ($CHCl_3$) and polar (H_2O) solvents (at T = 298 K and P = 1 bar). In Fig. 2(C), we observe that hierarchical structures of UPy dimers, stacked along their normal direction, form in both solvents with significantly higher aggregation propensity in water. A more detailed analysis of the monomers' mutual orientation during self-assembly shows that, in both solvents, dimer formation via DDAA arrangement is favored, along with growth along the stacking direction (see Fig. S4 and analysis details in supplementary material). The ordered configuration of such stacked assemblies is also confirmed by the radial distribution function (rdf) of the constituent UPy monomers in an assembled SP (Fig. S5). The rdf profile shows multiple regular peaks obtained at core–core distance. The first peak occurs at 0.37 nm, which identifies the first neighbors along the stacking direction. The next peak, located at ≈0.6 nm, corresponds to the monomer–monomer core distance relative to the planar dimer formation.

We thus apply our OPES-based approach to quantitatively assess cooperativity in the formation of such constructs. We first characterize the monomer–monomer binding via OPES, both in $CHCl_3$ and in water. We bias two CVs, the distance d between the centers of geometry of the monomers and the number (HB-dim) of dimerization-specific hydrogen bonds formed between the two monomers [Fig. 2(D), the CV detailed definition is given in Sec. IV]. By comparing the 2D free energy surfaces (FESs) obtained in the different solvents [Fig. 2(D)], we observe two diverse landscapes characterized by distinct global minima. In $CHCl_3$ the planar dimer configuration, corresponding to $d \approx 0.6$ nm and HB-dim ≈4 is by far the dominant state, whereas in water, this dimeric conformation becomes much less stable in favor of monomer π–π stacking (d = 0.37 nm). This, together with the outcomes of self-assembly MD, suggests that the polymerization dynamics are different in the two environments, as also supported by reported experimental and

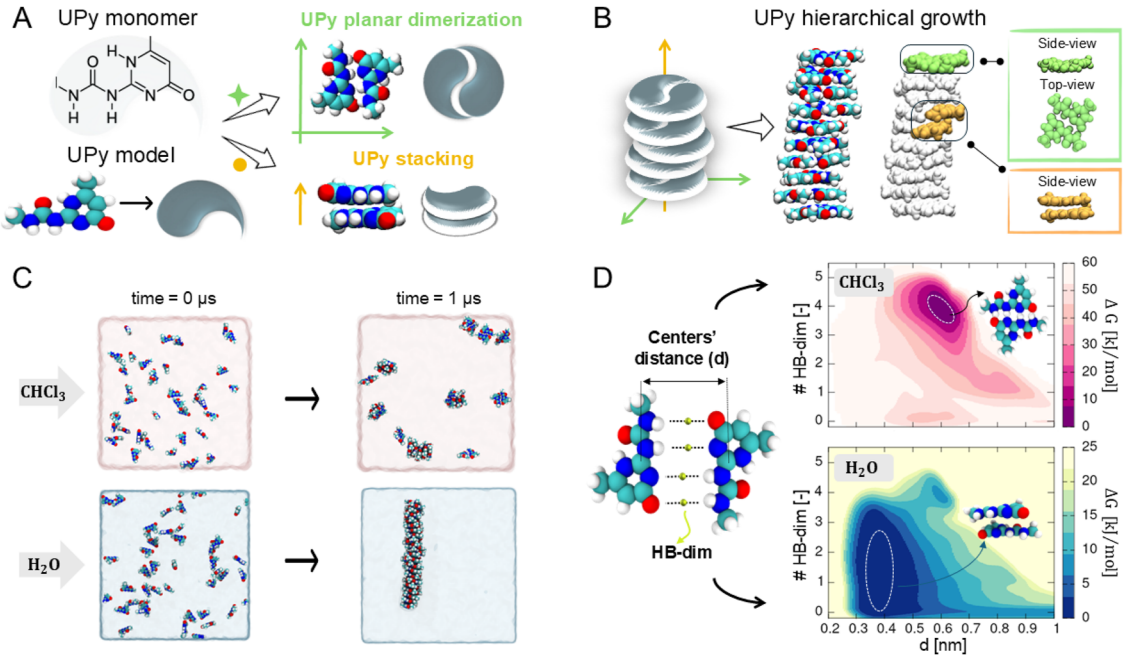

FIG. 2. Hierarchical assembly of UPy monomers. (A) UPy motif chemical formula and AA molecular model (left) and the two assembly modes of UPy-based monomers: dimerization and stacking (right). A cartoon representation of the monomer and its assembly modes is also shown. (B) Hierarchical formation of UPy SP via planar dimerization and stacking. (C) Self-assembly MD simulations of 42 UPy monomers in $CHCl_3$ (top) and H_2O (bottom). Snapshots at the beginning and after 1 μs of AA-MD are reported. Solvent molecules are not shown for clarity. (D) Free energy surface associated with UPy monomer binding/unbinding, as a function of two CVs: (i) the distance d between the centers of geometry of two UPy monomers and (ii) HB-dim, that is, the number of hydrogen bonds responsible for UPy dimerization (shown by dashed lines). In $CHCl_3$, the dimerization minimum is dominant, while in water, the global minimum corresponds to the stacking conformation, although dimerization remains relevant but less stable.

computational studies.[34,89,90] We therefore employed these first indications as a basis for the characterization of polymerization free energies.

We first focus on UPy polymerization in $CHCl_3$. As shown by Figs. 2(C) and 2(D), in this solvent, the equilibrium strongly favors the formation of planar dimers. We can therefore consider the HB-driven dimers as the fundamental unit toward SP formation, the stacking of which is the limiting step of the process [Fig. 3(A)].

To obtain insight into cooperativity, we focus on the conditional free energies of a *probe* dimer stacking onto a SP *template* of n dimers, namely $\Delta G_{2n,2}$. We underline that dimers can stack upon each other both in parallel and antiparallel fashions, as defined by the mutual orientation of normal vectors associated with the binding dimers [Fig. 3(B)]. Although none of these orientations has been shown to be strikingly favorable [Fig. S5(b)], for the sake of completeness, we consider two different types of templates, in which neighboring dimers are all in parallel or all in antiparallel configuration. As CV for the OPES-MD, we employ the minimum distance between the geometry centers of the probe dimer and the template's terminal dimers [Fig. 3(C)]. Such a CV choice disregards the orientation of the probe dimer, in fact averaging over all possible stacking modes, while remaining consistent with an estimate of the overall cooperativity of a considered polymerization step [Fig. 3(D)]. Moreover, consistently with the minimalistic CG models, we also overlook intercalation or branching events as sources of polymer growth since they have been shown to occur with lower incidence.[70] The resulting $\Delta G_{2n,2}$ profiles for the antiparallel template are shown in Fig. 3(E), while the $\Delta G_{2n,2}$ for the all-parallel template are reported in Fig. S6(d). All profiles present a clear free energy minimum for the stacked configuration, responsible for elongation of UPy polymers in $CHCl_3$. Binding free energies, evaluated as the difference in free energy between the bound (minimum) and an unbound state at the chosen distance d, exhibit a slightly anti-cooperative trend with the construct size [Fig. 3(F)], consistent with that previously observed in the **M** model [Fig. 1(E)]. This is compatible with a non-cooperative system with low elongation propensity [Fig. 2(C)]. No significant difference is found between parallel and antiparallel stacking [Fig. 3(F)].

In water, the binding free energy landscape [Fig. 2(D)] does not indicate a neat separation between the aggregation modes seen in $CHCl_3$. In aqueous solution, both aggregation modes can compete or cooperate toward polymerization, thereby defining a hierarchical growth that is not characterized by a precise stepwise self-assembly order [Fig. 4(A)]. We therefore apply OPES to estimate free energies associated with two different classes of polymerization steps: (i) $\Delta G_{2n,1}$, associated with the binding of a probe monomer on a template formed by n stacked dimers. This step can occur only via stacking, as all UPy dimers within the template are complete. (ii) $\Delta G_{2n+1,1}$, associated with the binding of a probe monomer on a template composed of n stacked dimers plus a monomer

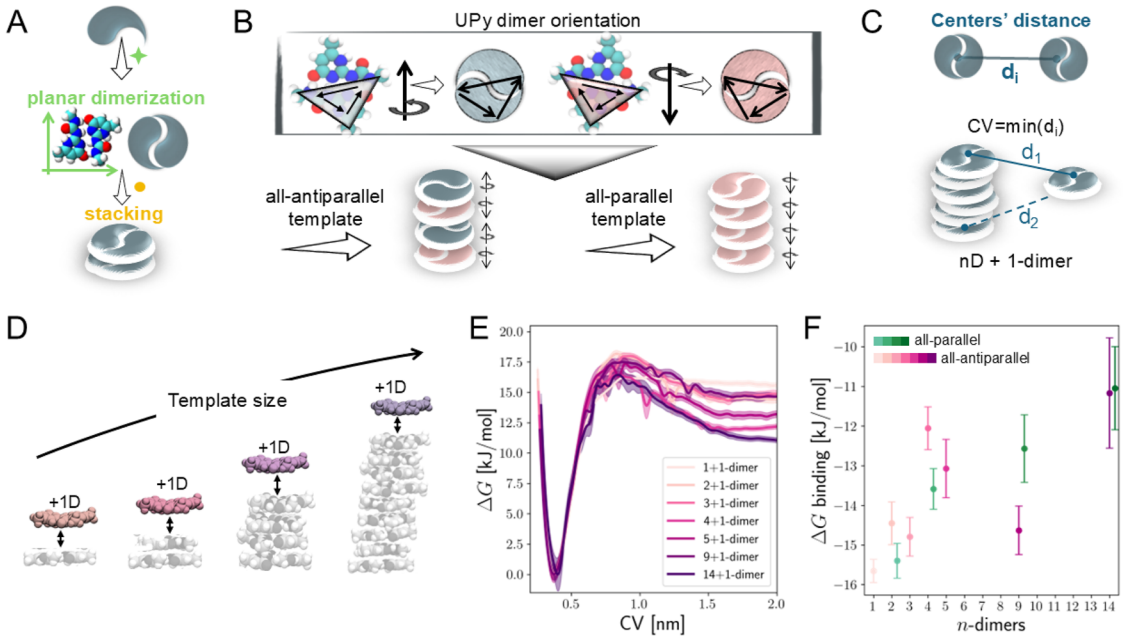

FIG. 3. Polymerization of UPy in $CHCl_3$. (A) Polymerization pathway of UPy in $CHCl_3$. Dimers are very stable [Fig. 2(D)], therefore the key process governing fiber formation is dimer stacking. (B) A normal vector to each UPy dimer defines its axial orientation. Based on this definition, the mutual arrangement of dimers can be either parallel or antiparallel. Cartoon representations of all-antiparallel and all-parallel SP templates are shown. (C) The minimum distance (d) between the geometric centers of terminal dimers is selected as CV for OPES simulations. (D) Scheme of the polymerization free energies based on a *probe* dimer stacking onto a *template* of n dimers ($\Delta G_{2n,2}$). (E) Free energy difference profiles as a function of the CV in all-antiparallel templates of increasing size n. (F) Dependence of binding free energy differences $\Delta G_{2n,2}$ on the template size n. Both all-antiparallel and all-parallel template results are shown. The free energy profiles for the all-parallel case are reported in Fig. S6.

individually stacked at one end. In this case, the monomer can either complete the dimer, undergoing simultaneous dimerization and stacking, or stack onto the single monomer (we prevent interaction with the other full-dimer terminal, see Sec. IV). In case (i), we apply OPES biasing a single CV, namely the minimum distance d between the geometric centers of the probe monomer and of the terminal dimers of the template stack [Fig. 4(B)]. We obtain the free energy profiles reported in Fig. 4(B), which indicate a slightly cooperative behavior of this polymerization step going from $n = 2$ to $n = 9$. In case (ii), as both aggregation modes are possible, we apply OPES biasing two CVs, in the same way as done for monomer–monomer binding characterization [Fig. 4(C)]. The 2D free energy surfaces obtained via these calculations show how the stacking minimum becomes shallower with size n, while the dimerization minimum becomes the favored state if compared with the FES of two UPy monomers in water (Fig. S8). The shift of the free energy global minimum from the stacking to the planar dimerization mode is even more evident after projecting the FES on the distance d [Fig. 4(D)]. The tendency to follow the hierarchical order, completing the dimers before growing longitudinally, is therefore favored in a cooperative way. Similarly to what was done for $CHCl_3$, we determined the difference between all-antiparallel (Fig. 4) and all-parallel templates, by testing the latter for $n = 9$. No relevant difference was found in the ΔG, as reported in Fig. 4(E) and Figs. S7(b)–S7(c).

The cooperative behavior of UPy SP growth in water, summarized in Fig. 4(E), reveals that both UPy polymerization modes follow a cooperative path, that is, ΔG of binding increases in modulo with polymer size.

III. DISCUSSION

In this study, we propose and apply a molecular simulation approach based on the OPES method to characterize the thermodynamics of supramolecular polymerization and obtain quantitative insight into supramolecular polymers' cooperativity. We first validated our approach with minimalistic CG models of SPs. We evaluated how polymerization free energies depend on the size of the interacting oligomers, highlighting the qualitatively different trends between an isodesmic and a cooperative model. We then extended the approach to the case of UPy-based SPs, characterized by a hierarchical aggregation pathway that combines two binding modes: hydrogen-bond-based dimerization and axial stacking. Our results show that in an apolar, $CHCl_3$ environment, the formation of hydrogen-bonded UPy dimers is strongly favorable, and stacking occurs between stable dimers. The polymer elongation in this case shows anticooperative character, promoting short over long constructs. In a polar H_2O solvent, the two aggregation modes are less thermodynamically separated; instead, they cooperate in the growth

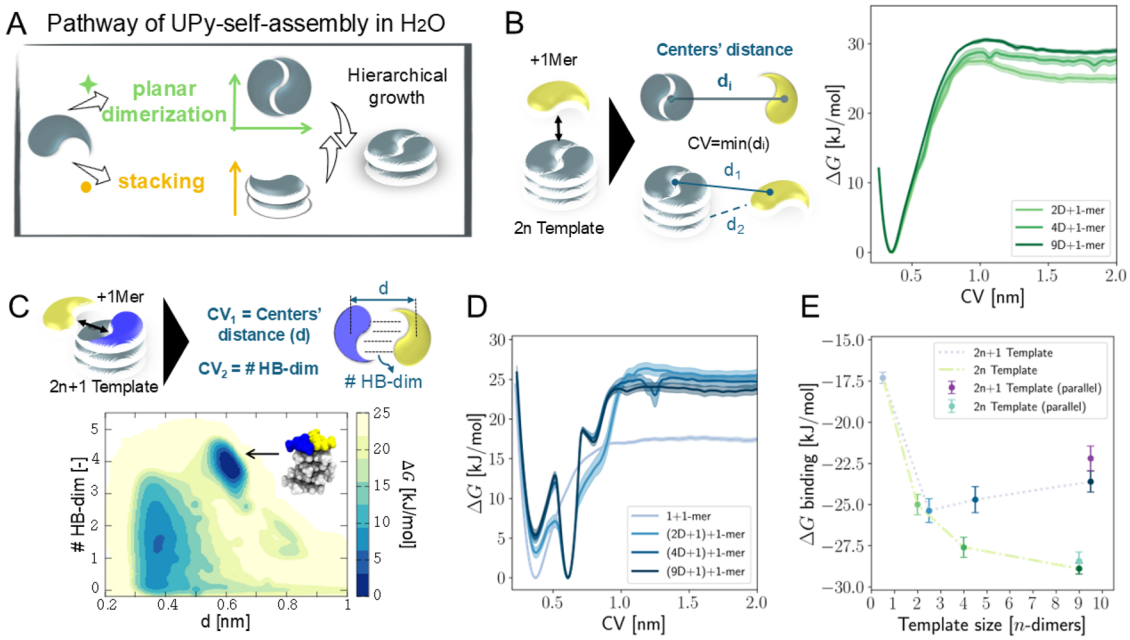

FIG. 4. Polymerization of UPy in H_2O. (A) The assembly of UPy monomers in water favors stacking, but planar dimerization is also relevant, indicating a polymerization landscape in which both modes cooperate toward fiber formation. We decompose the polymerization process by characterizing two steps: (i) the binding of a probe UPy monomer on a template of n stacked dimers ($\Delta G_{2n,1}$, left) and (ii) the binding of a monomer on a template stack of n dimers plus a stacked monomer ($\Delta G_{2n+1,1}$ right). (B) Step (i) is described by a single CV, namely the distance between the probe monomer and terminal dimer centers-of-geometry (left). The free energy differences $\Delta G_{2n,1}$ associated with the step (i) are shown as a function of this CV (right). (C) Step (ii) is described by two CVs, the distance between the centers of geometry of the probe monomer and the monomer at the template terminal, and the number of dimerization-specific hydrogen bonds formed between the two (left). 2D free energy profiles $\Delta G_{2n+1,1}$, with n = 4, associated with step (ii). (D) Projection of the free energy surfaces in C on the distance CV, d. (E) Free energy differences of binding associated with the two studied polymerization steps as a function of template size. The free energy differences for the all-parallel n = 9 cases are also shown (the respective profiles are reported in Fig. S7).

of UPy fibers. The free energies associated with different growth steps in water quantify how the presence of a template can reinforce both UPy polymerization modes, guiding the growth of the hierarchical fiber structure.

The proposed approach, leveraging the high-quality sampling offered by the OPES method, provides a robust framework to compute conditional polymerization free energies and precisely assess cooperativity. Such mechanistic insight is topical toward the rational design of supramolecular materials with tailored polymerization features.

IV. METHODS

A. Minimalistic models

The **M** monomer consists of seven beads of mass 72 u.m.a.: six arranged at the vertices of a hexagon and one central core bead [Fig. 1(A)], all connected via harmonic bonds. Nearest-neighbor beads are linked with a force constant of 20 000 kJ mol^{-1} nm^{-2} and an equilibrium length of 0.47 nm. Opposite vertex beads are also connected (force constant: 15 000 kJ mol^{-1} nm^{-2}, length: 0.94 nm) to ensure planarity. Non-bonded interactions between central beads follow a Lennard-Jones potential with σ = 0.47 nm and ε = 45 kJ mol^{-1} [Fig. 1(A)].

The $\mathbf{M}_{coop}$ model shares the hexagonal topology and bonded interactions of the **M** model, with the addition of a dipole vector centered on the core bead. This dipole consists of two oppositely charged material points ($q = \pm 1.4\ e$) fixed 0.28 nm apart (0.14 nm from the core), aligned via a harmonic angular potential (180°, force constant 1500 kJ mol^{-1}) [Fig. 1(B)]. The charged material points, with mass one-third that of regular beads, interact only via Coulomb forces and do not bear excluded volume, allowing the dipole to freely rotate and interact solely with other dipoles.

Both LJ and Coulomb interaction potentials are truncated and shifted at r_{cut} = 1.1 nm, to exclude, for simplicity, long-range effects on the assembly behavior of these minimalistic models. All OPES CG-MD simulations of the **M** and $\mathbf{M}_{coop}$ models were performed using GROMACS[91] coupled with PLUMED2[92,93] at a constant temperature T = 300 K, in a cubic volume of 6.2 nm per side, with periodic boundary conditions (PBC). The simulation of a generic polymerization step n-mer + m-mer starts from a pre-stacked perfect polymer of $n + m$ monomers. Harmonic wall restraints between the core beads of the first n monomers and of the remaining m monomers are applied to avoid breakage of the oligomers or permutation of their components (harmonic walls of k = 500 kJ mol^{-1} nm^{-2} at a core–core distance of 0.6 nm). The initial bond between the monomers n and $n + 1$ is instead

unrestrained to allow unbinding. Extra repulsive harmonic walls (k = 200 kJ mol^{-1} nm^{-2} at a core–core distance of 0.6 nm between chosen monomers) are used to prevent intercalation or branching of other monomers within the n-mer or m-mer backbone that could occur as a result of biasing.

The chosen CV for biasing is the minimum distance between all interacting ends of the n-mer and m-mer, calculated via the continuous function $\beta(\log\sum_i \exp\beta/d_i)^{-1}$, with β = 50. The OPES well-tempered sampling was performed,[58] with a kernel deposition frequency of 10 ps and a free energy barrier reference of 30 kJ mol^{-1}.

MD was simulated using Langevin equations (implicit solvent) via the `sd` integrator of GROMACS, with a 0.02 ps time step and friction constant γ = 10 ps^{-1}. Dimerization and elongation processes were run for 10^8 steps, while for coalescence, we used 20^8 steps.

Free energy profiles [Figs. 1(C) and 1(D)] were obtained by a reweighting procedure[58] after removing the initial 25% of the trajectory. The conditional free energy differences ΔF associated with the polymerization steps were estimated as the difference between the free energy minimum and the unbound free energy at s = 1.9 nm. The convergence of ΔF along the OPES simulation time is reported in Fig. S2. The spherical entropic correction $\delta F = +k_B T \log d^2$ is introduced to account for the symmetry of states. The internal energy (ΔU) and entropic ($-T\Delta S$) contributions (Fig. S1) were computed following Refs. 94 and 95.

Uncertainties in free energy, internal energy, and entropy profiles were estimated by combining reblocking and bootstrap analyses, as follows. The instantaneous uncertainties in the free energy [$F(s)$ or $G(s)$] and internal energy [$E(s)$] profiles were obtained from the fluctuations of the time-dependent free energy (or energy) estimates evaluated along the CV s. Because the time evolution of $F(s)$ [$G(s)$ and, to a lower extent, $E(s)$] is strongly correlated due to the dynamics of bias construction, we applied a reblocking analysis. To minimize assumptions about the underlying distribution, the block-averaged estimates were further resampled via bootstrapping; uncertainties were computed using 1000 bootstrap ensembles. By monitoring the dependence of the estimated uncertainty on the block size, we selected the optimal reblocking. Typical block sizes were of 5–10 ns for minimalistic MD simulations and of 20–30 ns for atomistic MD simulations. Uncertainties in the entropy profile and free energy differences (ΔF or ΔG) were propagated accordingly from the error estimates for free energy and internal energy profiles.

We underline that the obtained error bars can underestimate the uncertainty, as profile fluctuations along a single OPES trajectory are correlated by the biasing dynamics. This is the case in the estimates of internal energy differences in Fig. S1 and, as a consequence, of entropy differences, where profile fluctuations for unbound configurations (CV $\gtrsim$ 0.8 nm) are larger than the estimated error and more representative of the measurement uncertainty.

B. AA models of UPy SPs

The atomistic models of UPy-based monomers were built with the Avogadro.[96] Gaussian[97] tool, based on the HF/6-31G*, was used to estimate the generated electrostatic potential, and the RESP[98] method was then applied to obtain the partial charge distribution within the molecule. The complete parameterization was based on the General AMBER Force Field (GAFF),[99] using Antechamber.[100] The TIP3P[101] model is employed for water molecules, while the parameterization of $CHCl_3$ was carried out as described above for the UPy-based monomer. Nonbonded interactions, including van der Waals and short-range electrostatic interactions, were evaluated within a cutoff radius of 1.4 nm, while for the long-range electrostatics, particle-mesh Ewald summation was applied.

The self-assembly MD simulations of 42 UPy monomers in water and $CHCl_3$ were carried out with GROMACS.[91] The UPy monomers were randomly dispersed in a $10\times10\times10$ nm^3 box filled with solvent molecules. PBCs were applied in all directions. Two equilibration steps were performed to reach the thermodynamic conditions of 298 K and 10^5 Pa. The self-assembly simulation, lasting 1 μs, was then performed using a v-rescale thermostat[102] (τ_T = 0.1 ps) coupled with a c-rescale barostat[103] (τ_p = 2 ps).

1. OPES-MetaD simulations in AA simulations

For the OPES-based estimates of conditional free energy differences, we used the same MD settings employed in the AA self-assembly simulations. After the equilibration steps, we performed extensive 1 μs-long OPES-MetaD simulations[58] using GROMACS[91] and PLUMED2.[92,93] To study cooperativity, the following four distinct setups were considered:

- 1+1-mer: to explore the FES of two UPy monomers solvated either in water or $CHCl_3$;
- 2n+2-mer: to characterize the polymerization of a probe dimer on a template of n pre-stacked dimers in $CHCl_3$;
- 2n+1-mer: to characterize the polymerization of a probe 1-mer on a template of n pre-stacked dimers in water;
- (2n+1)+1-mer: to characterize the polymerization of a probe 1-mer on a terminal end having a single monomer stacked on a set of n pre-stacked dimers, highlighting the competition between stacking and planar dimerization modes.The FES in Fig. 2(D) shows the thermodynamic phase space of two UPy monomers interacting in $CHCl_3$ or aqueous solution (1+1-mer). To obtain the FES, we selected as CVs: (i) the core-core distance (d) between the geometric centers of the two UPy molecules, and (ii) the number HB-dim of dimerization-specific hydrogen bonds, estimated by computing the coordination number among the involved atoms (with a rational switching function, using $R_0 = 0.12D_0 = 0.27$[92,93]). The same CVs were also applied to investigate the (2n+1)+1-mer polymer growth in water [Fig. 4(C)]. Here, the simulations started from a pre-stacked polymer of n dimers + 1-mer, hold together by harmonic wall restraints to avoid polymer breakage. In particular, harmonic walls were imposed both on the HB-dim distances within the planar dimers and on the projection distances of each monomer on the polymer axes. Extra repulsive harmonic walls were used to prevent intercalation of the probe monomer within the backbone. For the polymerization cases 2n+2-mer and 2n+1-mer, the chosen CV for biasing was the minimum distance between the centers-of-geometry of the probe monomer and of the interacting terminals of the template n-dimer stack, calculated via the function $\beta(\log\sum_i \exp\beta/d_i)^{-1}$, with β = 50 to have a continuous function. The prestacked polymer of n dimers is held together by using the harmonic wall restraints described

above—same as the $(2n+1)$+1-mer case. The AA simulations carried out via OPES[58] well-tempered sampling were performed with a kernel deposition frequency of 100 ps and a free energy barrier reference of 30 kJ mol^{-1} in water and 50 kJ mol^{-1} in $CHCl_3$. Free energy profiles [Figs. 2(D), 3(D), 3(E), and 4(C)–(E)] were obtained by a reweighting procedure[58] after removing the initial 20% of the trajectory. The spherical entropic correction $\delta F = +k_B T \log d^2$ was introduced to correct along the distance CVs. This correction is not in fact present in the reported results, as we figured out during the revision process that it is not necessary (besides being in any case small enough, i.e. ~1.7 kJ/mol, to bear significant impact on the results). Errors are computed by combining reblocking and bootstrap analyses following the same procedure used for the minimalistic CG case. The effectiveness of the OPES procedure is highlighted by the sampling of numerous binding-unbinding events (see Figs. S9–S10) and by the satisfactory convergence of free energy differences, computed between the minimum configuration and a chosen unbound configuration (s = 1.9 nm), reported in Fig. S11.

SUPPLEMENTARY MATERIAL

The supplementary material features the following: (i) Free-energy decomposition and convergence plots for the minimalistic model simulations. (ii) Supplemental results and analyses for the AA-MD simulations of UPy polymerization, including an assessment of the side-chain effect, monomer/dimer orientation analyses, additional free-energy surfaces, the time evolution of CVs along the OPES-MD, and free-energy convergence plots. (iii) A summary of the computed binding free energies.

ACKNOWLEDGMENTS

C.P. acknowledges funding from the Italian Ministry of University and Research pursuant to Decree No. 23314 (Grant No. 11-12-2024)—BANDO FIS 2, SYSMAGRAD Project No. FIS-2023-00936. A.C. and D.P. acknowledge the European Union's Horizon Europe program under Grant Agreement No. 101192485 (ENDURION project). The authors acknowledge the computational resources provided by the Swiss National Supercomputing Center (CSCS).

AUTHOR DECLARATIONS

Conflict of Interest

The authors have no conflicts to disclose.

Author Contributions

A. Cardellini: Conceptualization (equal); Data curation (equal); Formal analysis (equal); Investigation (equal); Methodology (equal); Resources (equal); Software (equal); Validation (equal); Visualization (equal); Writing – original draft (equal); Writing – review & editing (equal). **D. Polino**: Conceptualization (supporting); Funding acquisition (equal); Methodology (supporting); Project administration (lead); Resources (equal); Writing – original draft (supporting); Writing – review & editing (supporting). **C. Perego**: Conceptualization (equal); Data curation (equal); Formal analysis (equal); Funding acquisition (equal); Investigation (equal); Methodology (equal); Software (equal); Supervision (lead); Validation (equal); Visualization (equal); Writing – original draft (equal); Writing – review & editing (equal).

DATA AVAILABILITY

The data that support the findings of this study are openly available in Zenodo at https://doi.org/10.5281/zenodo.18255749.[104]

REFERENCES

[1] J.-M. Lehn, Science **260**, 1762 (1993).
[2] L. Brunsveld, B. J. B. Folmer, E. W. Meijer, and R. P. Sijbesma, Chem. Rev. **101**, 4071 (2001).
[3] T. F. A. De Greef, M. M. J. Smulders, M. Wolffs, A. P. H. J. Schenning, R. P. Sijbesma, and E. W. Meijer, Chem. Rev. **109**, 5687 (2009).
[4] J.-M. Lehn, Prog. Polym. Sci. **30**, 814 (2005).
[5] X. Yan, F. Wang, B. Zheng, and F. Huang, Chem. Soc. Rev. **41**, 6042 (2012).
[6] R. Merindol and A. Walther, Chem. Soc. Rev. **46**, 5588 (2017).
[7] S. I. S. Hendrikse, S. P. W. Wijnands, R. P. M. Lafleur, M. J. Pouderoijen, H. M. Janssen, P. Y. W. Dankers, and E. W. Meijer, Chem. Commun. **53**, 2279 (2017).
[8] M. H. Bakker, C. C. Lee, E. W. Meijer, P. Y. W. Dankers, and L. Albertazzi, ACS Nano **10**, 1845 (2016).
[9] A. Mishra, D. B. Korlepara, M. Kumar, A. Jain, N. Jonnalagadda, K. K. Bejagam, S. Balasubramanian, and S. J. George, Nat. Commun. **9**, 1295 (2018).
[10] I. Insua, A. Cardellini, S. Díaz, J. Bergueiro, R. Capelli, G. M. Pavan, and J. Montenegro, Chem. Sci. **14**, 14074 (2023).
[11] S. Bernhard and M. W. Tibbitt, Adv. Drug Deliv. Rev. **171**, 240 (2021).
[12] Y. Cheng, E. Hirano, H. Wang, M. Kuwayama, E. W. Meijer, H. Huang, and T. Aida, Science **386**, 875 (2024).
[13] J. F. van Sprang, J. G. M. Aarts, M. G. T. A. Rutten, L. Rijns, B. M. Tiemeijer, M. J. G. Schotman, and P. Y. W. Dankers, Adv. Funct. Mater. **34**, 2404786 (2024).
[14] B. Zhu, Y. Cai, L. Zhou, L. Zhao, J. Chen, X. Shan, X. Sun, Q. You, X. Gong, W. Zhang *et al.*, Nat. Commun. **16**, 687 (2025).
[15] A. R. A. Palmans, J. A. J. M. Vekemans, E. E. Havinga, and E. W. Meijer, Angew Chem. Int. Ed. Engl. **36**, 2648 (1997).
[16] D. Zhao and J. S. Moore, Org. Biomol. Chem. **1**, 3471 (2003).
[17] J. D. Badjić, A. Nelson, S. J. Cantrill, W. B. Turnbull, and J. F. Stoddart, Acc. Chem. Res. **38**, 723 (2005).
[18] M. M. J. Smulders, A. P. H. J. Schenning, and E. W. Meijer, J. Am. Chem. Soc. **130**, 606 (2008).
[19] M. M. J. Smulders, M. M. L. Nieuwenhuizen, T. F. A. de Greef, P. van der Schoot, A. P. H. J. Schenning, and E. W. Meijer, Chem. - Eur. J. **16**, 362 (2010).
[20] A. Sorrenti, J. Leira-Iglesias, A. J. Markvoort, T. F. A. de Greef, and T. M. Hermans, Chem. Soc. Rev. **46**, 5476 (2017).
[21] D. B. Korlepara, W. R. Henderson, R. K. Castellano, and S. Balasubramanian, Chem. Commun. **55**, 3773 (2019).
[22] S. Ogi, K. Sugiyasu, S. Manna, S. Samitsu, and M. Takeuchi, Nat. Chem. **6**, 188 (2014).
[23] J. Gershberg, F. Fennel, T. H. Rehm, S. Lochbrunner, and F. Würthner, Chem. Sci. **7**, 1729 (2016).
[24] K. Cai, J. Xie, D. Zhang, W. Shi, Q. Yan, and D. Zhao, J. Am. Chem. Soc. **140**, 5764 (2018).
[25] Y. Dorca, C. Naranjo, G. Ghosh, B. Soberats, J. Calbo, E. Ortí, G. Fernández, and L. Sánchez, Chem. Sci. **13**, 81 (2022).
[26] V. Simic, L. Bouteiller, and M. Jalabert, J. Am. Chem. Soc. **125**, 13148 (2003).

[27] M. M. J. Smulders, I. A. W. Filot, J. M. A. Leenders, P. van der Schoot, A. R. A. Palmans, A. P. H. J. Schenning, and E. W. Meijer, J. Am. Chem. Soc. **132**, 611 (2010).
[28] M. Endo, T. Fukui, S. H. Jung, S. Yagai, M. Takeuchi, and K. Sugiyasu, J. Am. Chem. Soc. **138**, 14347 (2016).
[29] S. Ogi, T. Fukui, M. L. Jue, M. Takeuchi, and K. Sugiyasu, Angew. Chem. Int. Ed. **53**, 14363 (2014).
[30] S. Ogi, V. Stepanenko, K. Sugiyasu, M. Takeuchi, and F. Würthner, J. Am. Chem. Soc. **137**, 3300 (2015).
[31] P. A. Korevaar, S. J. George, A. J. Markvoort, M. M. J. Smulders, P. A. J. Hilbers, A. P. H. J. Schenning, T. F. A. De Greef, and E. W. Meijer, Nature **481**, 492 (2012).
[32] L. H. Beun, L. Albertazzi, D. van der Zwaag, R. de Vries, and M. A. Cohen Stuart, ACS Nano **10**, 4973 (2016).
[33] N. M. Casellas, S. Pujals, D. Bochicchio, G. M. Pavan, T. Torres, L. Albertazzi, and M. García-Iglesias, Chem. Commun. **54**, 4112 (2018).
[34] P. A. Korevaar, C. Schaefer, T. F. A. de Greef, and E. W. Meijer, J. Am. Chem. Soc. **134**, 13482 (2012).
[35] L. Albertazzi, F. J. Martinez-Veracoechea, C. M. A. Leenders, I. K. Voets, D. Frenkel, and E. W. Meijer, Proc. Natl. Acad. Sci. **110**, 12203 (2013).
[36] L. Albertazzi, D. van der Zwaag, C. M. A. Leenders, R. Fitzner, R. W. van der Hofstad, and E. W. Meijer, Science **344**, 491 (2014).
[37] A. Aliprandi, M. Mauro, and L. De Cola, Nat. Chem. **8**, 10 (2016).
[38] X. Lou, R. P. M. Lafleur, C. M. A. Leenders, S. M. C. Schoenmakers, N. M. Matsumoto, M. B. Baker, J. L. J. van Dongen, A. R. A. Palmans, and E. W. Meijer, Nat. Commun. **8**, 15420 (2017).
[39] B. Adelizzi, A. Aloi, N. J. Van Zee, A. R. A. Palmans, E. W. Meijer, and I. K. Voets, ACS Nano **12**, 4431 (2018).
[40] A. Sarkar, R. Sasmal, C. Empereur-mot, D. Bochicchio, S. V. K. Kompella, K. Sharma, S. Dhiman, B. Sundaram, S. S. Agasti, G. M. Pavan, and S. J. George, J. Am. Chem. Soc. **142**, 7606 (2020).
[41] H. Su, S. A. H. Jansen, T. Schnitzer, E. Weyandt, A. T. Rösch, J. Liu, G. Vantomme, and E. W. Meijer, J. Am. Chem. Soc. **143**, 17128 (2021).
[42] K. K. Bejagam, G. Fiorin, M. L. Klein, and S. Balasubramanian, J. Phys. Chem. B **118**, 5218 (2014).
[43] F. Tantakitti, J. Boekhoven, X. Wang, R. V. Kazantsev, T. Yu, J. Li, E. Zhuang, R. Zandi, J. H. Ortony, C. J. Newcomb, L. C. Palmer, G. S. Shekhawat, M. O. de la Cruz, G. C. Schatz, and S. I. Stupp, Nat. Mater. **15**, 469 (2016).
[44] X. Li, J. Lai, Y. Deng, J. Song, G. Zhao, and S. Dong, J. Am. Chem. Soc. **142**, 21522 (2020).
[45] O.-S. Lee, V. Cho, and G. C. Schatz, Nano Lett. **12**, 4907 (2012).
[46] K. K. Bejagam and S. Balasubramanian, J. Phys. Chem. B **119**, 5738 (2015).
[47] D. Bochicchio and G. M. Pavan, ACS Nano **11**, 1000 (2017).
[48] M. B. Baker, L. Albertazzi, I. K. Voets, C. M. A. Leenders, A. R. A. Palmans, G. M. Pavan, and E. W. Meijer, Nat. Commun. **6**, 6234 (2015).
[49] M. Garzoni, M. B. Baker, C. M. A. Leenders, I. K. Voets, L. Albertazzi, A. R. A. Palmans, E. W. Meijer, and G. M. Pavan, J. Am. Chem. Soc. **138**, 13985 (2016).
[50] D. Bochicchio and G. M. Pavan, J. Phys. Chem. Lett. **8**, 3813 (2017).
[51] A. L. de Marco, D. Bochicchio, A. Gardin, G. Doni, and G. M. Pavan, ACS Nano **15**, 14229 (2021).
[52] S. H. Jung, D. Bochicchio, G. M. Pavan, M. Takeuchi, and K. Sugiyasu, J. Am. Chem. Soc. **140**, 10570 (2018).
[53] C. Perego, L. Pesce, R. Capelli, S. J. George, and G. M. Pavan, ChemSystemsChem **3**, e2000038 (2021).
[54] M. Crippa, C. Perego, A. L. de Marco, and G. M. Pavan, Nat. Commun. **13**, 2162 (2022).
[55] E. Weyandt, L. Leanza, R. Capelli, G. M. Pavan, G. Vantomme, and E. W. Meijer, Nat. Commun. **13**, 248 (2022).
[56] F. Baftizadeh, F. Pietrucci, X. Biarnés, and A. Laio, Phys. Rev. Lett. **110**, 168103 (2013).
[57] D. Bochicchio, M. Salvalaglio, and G. M. Pavan, Nat. Commun. **8**, 147 (2017).
[58] M. Invernizzi and M. Parrinello, J. Phys. Chem. Lett. **11**, 2731 (2020).
[59] M. Crippa, C. Perego, and G. M. Pavan, Nat. Commun. **16**, 5030 (2025).
[60] R. P. Sijbesma, F. H. Beijer, L. Brunsveld, B. J. B. Folmer, J. H. K. K. Hirschberg, R. F. M. Lange, J. K. L. Lowe, and E. W. Meijer, Science **278**, 1601 (1997).
[61] F. H. Beijer, R. P. Sijbesma, H. Kooijman, A. L. Spek, and E. W. Meijer, J. Am. Chem. Soc. **120**, 6761 (1998).
[62] P. Y. W. Dankers, M. C. Harmsen, L. A. Brouwer, M. J. A. Van Luyn, and E. W. Meijer, Nat. Mater. **4**, 568 (2005).
[63] A. F. Vrehen, J. F. van Sprang, M. J. G. Schotman, and P. Y. W. Dankers, Mater. Today Bio **26**, 101021 (2024).
[64] L. Rijns, M. B. Baker, and P. Y. W. Dankers, J. Am. Chem. Soc. **146**, 17539 (2024).
[65] C. M. Wallace, M. M. Rovers, R. Bellan, M. G. T. A. Rutten, A. Seddon, M. J. Dalby, P. Y. W. Dankers, and D. J. Adams, J. Mater. Chem. B **12**, 9283 (2024).
[66] H. Fu, J. Huang, J. J. B. van der Tol, L. Su, Y. Wang, S. Dey, P. Zijlstra, G. Fytas, G. Vantomme, P. Y. W. Dankers, and E. W. Meijer, Nature **626**, 1011 (2024).
[67] L. Rijns, J. W. Peeters, S. I. S. Hendrikse, M. E. J. Vleugels, X. Lou, H. M. Janssen, E. W. Meijer, and P. Y. W. Dankers, Chem. Mater. **35**, 8203 (2023).
[68] L. Rijns, M. G. T. A. Rutten, R. Bellan, H. Yuan, M. L. Mugnai, S. Rocha, E. del Gado, P. H. J. Kouwer, and P. Y. W. Dankers, Sci. Adv. **10**, eadr3209 (2024).
[69] A. Barducci, G. Bussi, and M. Parrinello, Phys. Rev. Lett. **100**, 020603 (2008).
[70] A. Cardellini, C. Caruso, L. Rijns, P. Y. W. Dankers, G. M. Pavan, and C. Perego, J. Mater. Chem. B **13**, 14326 (2025).
[71] R. F. Goldstein and L. Stryer, Biophys. J. **50**, 583 (1986).
[72] A. J. Markvoort, H. M. M. ten Eikelder, P. A. J. Hilbers, T. F. A. de Greef, and E. W. Meijer, Nat. Commun. **2**, 509 (2011).
[73] A. J. Markvoort, H. M. M. ten Eikelder, P. A. J. Hilbers, and T. F. A. de Greef, ACS Cent. Sci. **2**, 232 (2016).
[74] M. M. J. Smulders, M. M. L. Nieuwenhuizen, M. Grossman, I. A. W. Filot, C. C. Lee, T. F. A. de Greef, A. P. H. J. Schenning, A. R. A. Palmans, and E. W. Meijer, Macromolecules **44**, 6581 (2011).
[75] T. C. Michaels, A. Šarić, J. Habchi, S. Chia, G. Meisl, M. Vendruscolo, C. M. Dobson, and T. P. Knowles, Annu. Rev. Phys. Chem. **69**, 273 (2018).
[76] H. M. M. ten Eikelder and A. J. Markvoort, Acc. Chem. Res. **52**, 3465 (2019).
[77] M. Becchi, R. Capelli, C. Perego, G. M. Pavan, and C. Micheletti, Soft Matter **18**, 8106 (2022).
[78] E. Rossi, A. Ferrarini, and M. Sulpizi, Phys. Chem. Chem. Phys. **25**, 6102 (2023).
[79] E. Darve, D. Rodríguez-Gómez, and A. Pohorille, J. Chem. Phys. **128**, 144120 (2008).
[80] A. Sharko, D. Livitz, S. De Piccoli, K. J. M. Bishop, and T. M. Hermans, Chem. Rev. **122**, 11759 (2022).
[81] L. Brunsveld, H. Zhang, M. Glasbeek, J. A. J. M. Vekemans, and E. W. Meijer, J. Am. Chem. Soc. **122**, 6175 (2000).
[82] M. F. J. Mabesoone, A. J. Markvoort, M. Banno, T. Yamaguchi, F. Helmich, Y. Naito, E. Yashima, A. R. A. Palmans, and E. W. Meijer, J. Am. Chem. Soc. **140**, 7810 (2018).
[83] S. Datta, Y. Kato, S. Higashiharaguchi, K. Aratsu, A. Isobe, T. Saito, D. D. Prabhu, Y. Kitamoto, M. J. Hollamby, A. J. Smith, R. Dalgliesh, N. Mahmoudi, L. Pesce, C. Perego, G. M. Pavan, and S. Yagai, Nature **583**, 400 (2020).
[84] J. Comer, J. C. Gumbart, J. Hénin, T. Lelièvre, A. Pohorille, and C. Chipot, J. Phys. Chem. B **119**, 1129 (2015).
[85] J. Hénin, G. Fiorin, C. Chipot, and M. L. Klein, J. Chem. Theory Comput. **6**, 35 (2010).
[86] R. Bellan, A. Cardellini, C. Perego, L. J. M. M. Paffen, L. Rijns, G. M. Pavan, and P. Y. W. Dankers, J. Polym. Sci. **2025**, 1–9.
[87] D. J. M. van Beek, A. J. H. Spiering, G. W. M. Peters, K. te Nijenhuis, and R. P. Sijbesma, Macromolecules **40**, 8464 (2007).
[88] W. P. J. Appel, G. Portale, E. Wisse, P. Y. W. Dankers, and E. W. Meijer, Macromolecules **44**, 6776 (2011).
[89] S. Nandi, S. Behera, and C. Kulkarni, Angew. Chem. Int. Ed. **64**, e202424138 (2025).
[90] R. Bobrovs, L. Drunka, A. A. Auzins, K. Jaudzems, and M. Salvalaglio, Cryst. Growth Des. **21**, 436 (2021).
[91] M. J. Abraham, T. Murtola, R. Schulz, S. Páll, J. C. Smith, B. Hess, and E. Lindahl, SoftwareX **1–2**, 19 (2015).
[92] M. Bonomi, D. Branduardi, G. Bussi, C. Camilloni, D. Provasi, P. Raiteri, D. Donadio, F. Marinelli, F. Pietrucci, R. A. Broglia, and M. Parrinello, Comput. Phys. Commun. **180**, 1961 (2009).

[93]G. A. Tribello, M. Bonomi, D. Branduardi, C. Camilloni, and G. Bussi, Comput. Phys. Commun. **185**, 604 (2014).
[94]I. Gimondi, G. A. Tribello, and M. Salvalaglio, J. Chem. Phys. **149**, 104104 (2018).
[95]L. Kollias, D. C. Cantu, V.-A. Glezakou, R. Rousseau, and M. Salvalaglio, Adv. Theory Simul. **3**, 2000092 (2020).
[96]M. D. Hanwell, D. E. Curtis, D. C. Lonie, T. Vandermeersch, E. Zurek, and G. R. Hutchison, J. Cheminform. **4**, 17 (2012).
[97]M. J. Frisch, G. W. Trucks, H. B. Schlegel, G. E. Scuseria, M. A. Robb, J. R. Cheeseman, G. Scalmani, V. Barone, G. A. Petersson, H. Nakatsuji, X. Li, M. Caricato, A. V. Marenich, J. Bloino, B. G. Janesko, R. Gomperts, B. Mennucci, H. P. Hratchian, J. V. Ortiz, A. F. Izmaylov, J. L. Sonnenberg, D. Williams-Young, F. Ding, F. Lipparini, F. Egidi, J. Goings, B. Peng, A. Petrone, T. Henderson, D. Ranasinghe, V. G. Zakrzewski, J. Gao, N. Rega, G. Zheng, W. Liang, M. Hada, M. Ehara, K. Toyota, R. Fukuda, J. Hasegawa, M. Ishida, T. Nakajima, Y. Honda, O. Kitao, H. Nakai, T. Vreven, K. Throssell, J. A. Montgomery, Jr., J. E. Peralta, F. Ogliaro, M. J. Bearpark, J. J. Heyd, E. N. Brothers, K. N. Kudin, V. N. Staroverov, T. A. Keith, R. Kobayashi, J. Normand, K. Raghavachari, A. P. Rendell, J. C. Burant, S. S. Iyengar, J. Tomasi, M. Cossi, J. M. Millam, M. Klene, C. Adamo, R. Cammi, J. W. Ochterski, R. L. Martin, K. Morokuma, O. Farkas, J. B. Foresman, and D. J. Fox, *Gaussian 16, Revision C.01*, Gaussian, Inc., Wallingford, CT, 2016.
[98]C. I. Bayly, P. Cieplak, W. Cornell, and P. A. Kollman, J. Phys. Chem. **97**, 10269 (1993).
[99]J. Wang, R. M. Wolf, J. W. Caldwell, P. A. Kollman, and D. A. Case, J. Comput. Chem. **25**, 1157 (2004).
[100]J. Wang, W. Wang, P. A. Kollman, and D. A. Case, J. Mol. Graphics Modell. **25**, 247 (2006).
[101]P. Mark and L. Nilsson, J. Phys. Chem. A **105**, 9954 (2001).
[102]G. Bussi, D. Donadio, and M. Parrinello, J. Chem. Phys. **126**, 014101 (2007).
[103]M. Bernetti and G. Bussi, J. Chem. Phys. **153**, 114107 (2020).
[104]A. Cardellini, D. Polino, and C. Perego (2026). "Research data supporting: Supramolecular cooperativity through the lens of enhanced sampling molecular dynamics," Zenodo. https://doi.org/10.5281/zenodo.18255749